IEEE Access
Multidisciplinary | Rapid Review | Open Access Journal

Received July 12, 2019, accepted July 30, 2019, date of publication August 6, 2019, date of current version August 21, 2019.

*Digital Object Identifier 10.1109/ACCESS.2019.2933469*

# An AC–DC Hybrid Multi-Port Energy Router With Coordinated Control and Energy Management Strategies

**BIN LIU[1], WEIHAN WU[1], CHUNXIAO ZHOU[1], CHENGXIONG MAO[1], (Senior Member, IEEE), DAN WANG[1], (Senior Member, IEEE), QING DUAN[2], AND GUANGLIN SHA[2]**

[1]State Key Laboratory of Advanced Electromagnetic Engineering and Technology, Hubei Electric Power Security and High Efficiency Key Laboratory, School of Electrical and Electronic Engineering, Huazhong University of Science and Technology, Wuhan 430074, China
[2]Beijing Key Laboratory of Distribution Transformer Energy-Saving Technology, China Electric Power Research Institute, Beijing 100192, China

Corresponding author: Chengxiong Mao (cxmao@hust.edu.cn)

This work was supported by the Nation Basic Research Program of China under Grant 2015CB251301.

**ABSTRACT** Energy router is an intelligent power electronic device that can realize the active management of power flow and provide convenient access to distributed energy resource. This paper presents the structure of an AC-DC hybrid multi-port energy router, which acts as the interface between the power consumer and the distribution network. The corresponding coordinated control strategy is developed to guarantee the regular operation of the energy router and a mode switch strategy with advanced compensation is proposed to achieve seamless transition between grid-connected mode and islanded mode. A novel and practical fuzzy logic controller considering unit-time electricity charge is proposed for the energy router to prolong battery life, to improve economic benefits of power consumers, and to smooth fluctuations of renewable energy generation or load consumption. The simulation and experimental results have validated the coordinated control and energy management strategies and demonstrated that the energy router has satisfactory performance.

**INDEX TERMS** Energy router, distribution power system, energy storage, fuzzy control, coordinated control strategy, energy management.

## I. INTRODUCTION

Recently, due to the shortage of fossil energy and the demand for sustainable development, much attention has been paid to the development and utilization of renewable energy resource. The concept of energy internet (EI) [1] has been widely concerned, which is aimed to build a new intelligent system with the integration of distributed energy resource (DER) and the existing smart grid [2]. With the rapid increase of DERs in the power system, if large-scale DERs access to the distribution network dispersedly, it will have a severe impact on the security and quality of network operation in view of the decentralization, randomness, and intermittence of DERs. Meanwhile, multiform and high-reliable power supply is required to satisfy the demands of power consumers, which is a difficulty for traditional distribution network [3]. In order to solve these problems, the concept of energy router (ER) [4] is proposed.

ER, also called power router [5] and digital grid router [6], is the key equipment to build the EI [7]. The structure of ER is developed from solid state transformer (SST) [8]. Based on the functions of SST, ERs also need to achieve the intelligent management and real-time communication of the smart grid, DERs, and loads. Benefiting from the progress in power electronics and communication technology, ERs are developing rapidly and showing attractive features in power quality control [9], AC-DC hybrid distribution [10], active management of bidirectional power flows [11], convenient access to DERs [12], [13], energy management optimization [14], [15], etc. It appears that ERs can play an important role in the future smart grid.

In view of the expensive cost and large volume of the whole device, it will take a long time for ERs to be widely used in high-voltage distribution network. However, there

The associate editor coordinating the review of this manuscript and approving it for publication was Yijie Wang.

already have practical application prospects for ERs in low-voltage distribution network. For power consumers in low-voltage load areas (e.g., households, companies, farms), more requirements for power supply are put forward, including high power supply reliability, high power quality, and various forms of electric energy. Moreover, with the development of DERs, power consumers can be not only consumers but also producers [6]. The application of ERs in low-voltage distribution network will meet the demands of power consumers, and make full use of DER to achieve economic benefits.

Some literatures have investigated the application of ER in low-voltage distribution network in recent years. Literature [16] proposed a multiple hierarchic structure of the fully flexible power distribution system based on ERs, and pointed out that ERs will be the key equipment for building the EI. Literature [17] presented an ER-based interconnecting framework for microgrids with the consideration of energy complements between different microgrids. Literature [18] introduced a multiple microgrids framework constructed by an ER and proposed the corresponding control strategy including trading mechanism and price stimulation mechanism. However, the structures presented in [16]–[18] lack the support of experimental results. Literature [10] introduced the design and implementation of a multi-port ER of which the performance was verified by experiments. Literature [19] introduced a household ER that is suitable for low-voltage and small-capacity load area and presented the corresponding mathematical model and control strategy. Literature [20] discussed the different operation modes of the ER and validate the design of a single phase ER by simulations and experimental results. Nevertheless, no energy storage device is included in the ERs presented in [10], [19], and [20], and there is no discussion on the energy management strategy of ERs. Considering that the energy storage device can support the regular operation of ERs in islanded mode and achieve energy distribution optimization in grid-connected mode, the energy storage device should be an essential component of ERs, and it is necessary to study the energy management strategy that is suitable for ERs in low-voltage distribution network.

Based on ERs, a hybrid energy system integrating DERs and energy storage devices can be developed. Literatures [21], [22] give the review of energy management strategies for hybrid energy system. Hereinto, fuzzy logic controller (FLC) has been shown to be an effective and uncomplicated solution for solving multi-objective problems, which is appropriate for energy management design of ERs. Generally, the state of charge (SOC) of battery and net power flow are chosen as the two input variables of FLC for hybrid renewable energy system [23]–[26]. However, the electricity price is neglected in the design of FLC in [23]–[26], which should be a major consideration for ERs in low-voltage distribution network because power consumers attach great importance to economic benefits. Literature [27] employs electricity price as the third input variable of FLC to minimize the operational cost. Nevertheless, a FLC with three input variables is complicated in design and calculation, which is not suitable for actual device.

In this paper, an AC-DC hybrid multi-port energy router (MER) is presented for low-voltage small-capacity areas, which acts as the interface between the power consumer and the distribution network. The operation modes of the MER are classified, and the coordinated control strategy is developed for the MER to ensure the regular operation under different modes. A mode switch strategy with advanced compensation is proposed to achieve seamless transition between grid-connected mode and islanded mode. A FLC considering unit-time electricity charge is proposed for the MER to obtain the desired charging/discharging state of energy battery in grid-connected mode, which is a comprehensive optimization solution for prolonging battery life, improving economic benefits of power consumers, and smoothing fluctuations of renewable energy generation or load consumption. The simulation and experimental results have validated the proposed coordinated control and energy management strategies, showing that the MER has satisfactory performance.

## II. CONCEPT OF MER

### A. MER-BASED ENERGY SUBNET

In this paper, the term ''energy subnet'' is used to describe the system constructed by the MER, which is oriented to power consumers in low-voltage distribution network. The MER-based energy subnet consists of the MER, distribution grid, energy storage (ES) battery, distributed generation (DG), distributed energy storage (DES), load, microgrid, and intelligent power switch (IPS). Fig. 1 shows the framework of MER-based energy subnet, where the MER is the key equipment to achieve the operation control and energy management of the energy subnet.

As shown in Fig. 1, the MER provides five ports, namely Port 1-5, respectively. Port 1 is connected to the

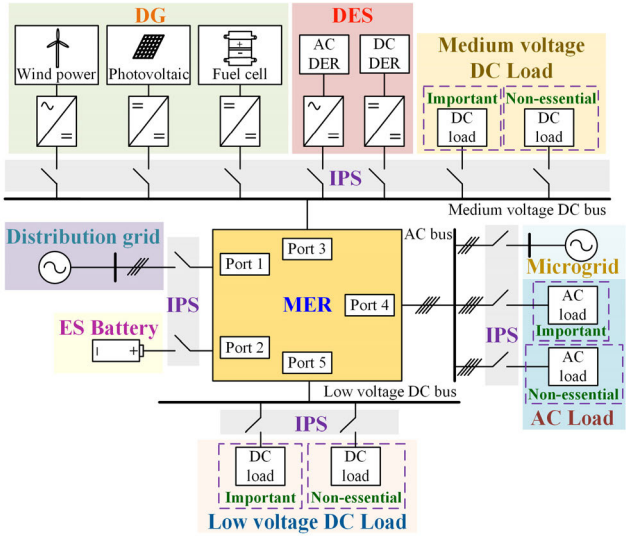


**FIGURE 1.** Framework of MER-based energy subnet.

distribution grid and can achieve bidirectional power flow. Port 2 is connected to an ES battery for energy management. Port 3 provides a medium voltage (MV) DC bus that gives access to uncontrollable DGs (e.g., photovoltaic and wind power), controllable DGs (e.g., fuel cell), DESs, and MV DC loads (e.g., electrical vehicle). Port 4 can supply power for AC loads or access to a microgrid. Port 5 can supply power for low voltage (LV) DC loads.

The energy subnet framework presented in Fig. 1 is very suitable for low-voltage distribution network, and its attractive characteristics are as follows:

1) Based on the MER, power consumers can obtain AC-DC hybrid power in multiple voltage levels. Though only three buses are shown in Fig. 1 for the sake of brevity, the MER can provide more AC and DC buses in different voltage levels according to the actual need.

2) A common MV dc bus is provided for the plug-and-play access of DGs and DESs. In this way, the structure and control can be greatly simplified for converters of DGs and DERs, since there is no need for these converters to consider the grid-connection problem.

3) The energy subnet can be controlled and managed uniformly by the MER with high integration of information flow and electric power flow. The fault and interference between the grid side and the user side are isolated by the MER. When the distribution grid fails, the regular operation of the energy subnet can be maintained by the ES battery, thus the power supply reliability can be guaranteed.

### B. MER STRUCTURE

As shown in Fig. 2, the MER consists of five parts: grid-connected part, ES part, MV DC part, AC part, and LV DC part. Considering the application of MER for power consumers in low-voltage distribution network, no isolation transformer is used between grid-connected part and AC part, so as to reduce the device volume and cost.

In the MER, grid-connected part is composed of a filter and an AC/DC converter to realize bidirectional power flow between a 380 V distribution grid and the MER. ES part comprises a DC/DC converter and filter inductance, and it is an essential part to achieve the energy management and high power supply reliability. MV DC part consists of some support capacitors, and supplies 750 V DC port which can realize the access of DGs, DESs, and loads. AC part consists of a DC/AC converter and filters, which is in charge of providing three-phase four-wire 380 V AC output for loads or connecting to a microgrid. LV DC part is made up of a DC/DC converter (or a DC/AC/AC/DC converter) and filters to supply 48 V DC power.

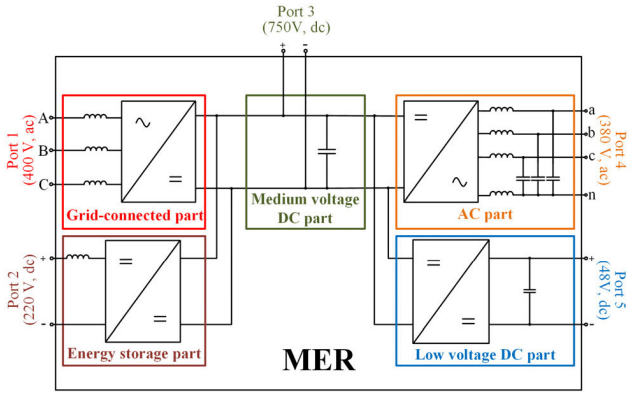


**FIGURE 2.** Structure of MER.

## III. CONTROL STRATEGY OF MER

It is the most basic requirement for the MER to ensure regular operation and realize reliable power supply. Since the MER can operate in different modes, corresponding control strategies should be employed based on the operation modes.

### A. OPERATION MODE CLASSIFICATION

For the MER, there are four operation modes, including standby mode, grid-connected mode, islanded mode, and fault mode. The transition relationships between these operation modes are shown in Fig. 3. Grid-connected mode and islanded mode are corresponding to the situation when the MER is working, while standby mode and fault mode are corresponding to the situation when the MER is halted.

In standby mode, the MER pauses and waits a start command. After startup process, the MER will work in grid-connected mode if the distribution grid is normal, or in islanded mode if the distribution grid fails.

In grid-connected mode, the port of grid-connected part is connected to the distribution grid, and the controller of grid-connected part is responsible for the voltage stability of MV DC link. The controller of ES part is aimed to obtain the desired charging/discharging state of energy battery, according to the designed energy management strategy.

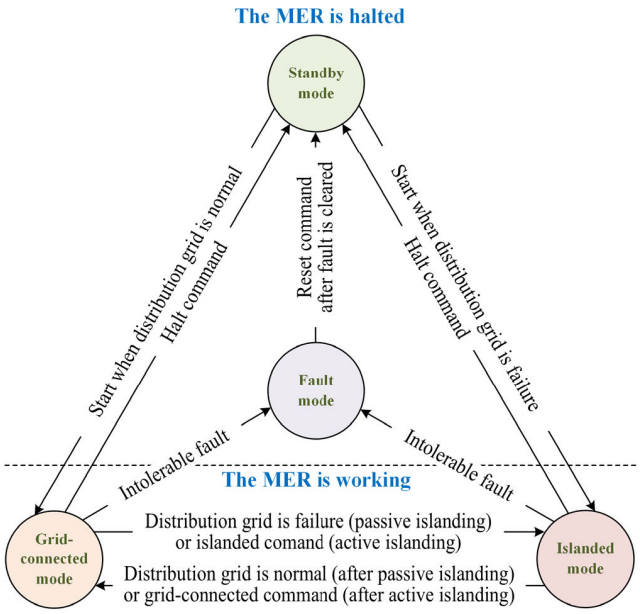


**FIGURE 3.** Operation mode transition.

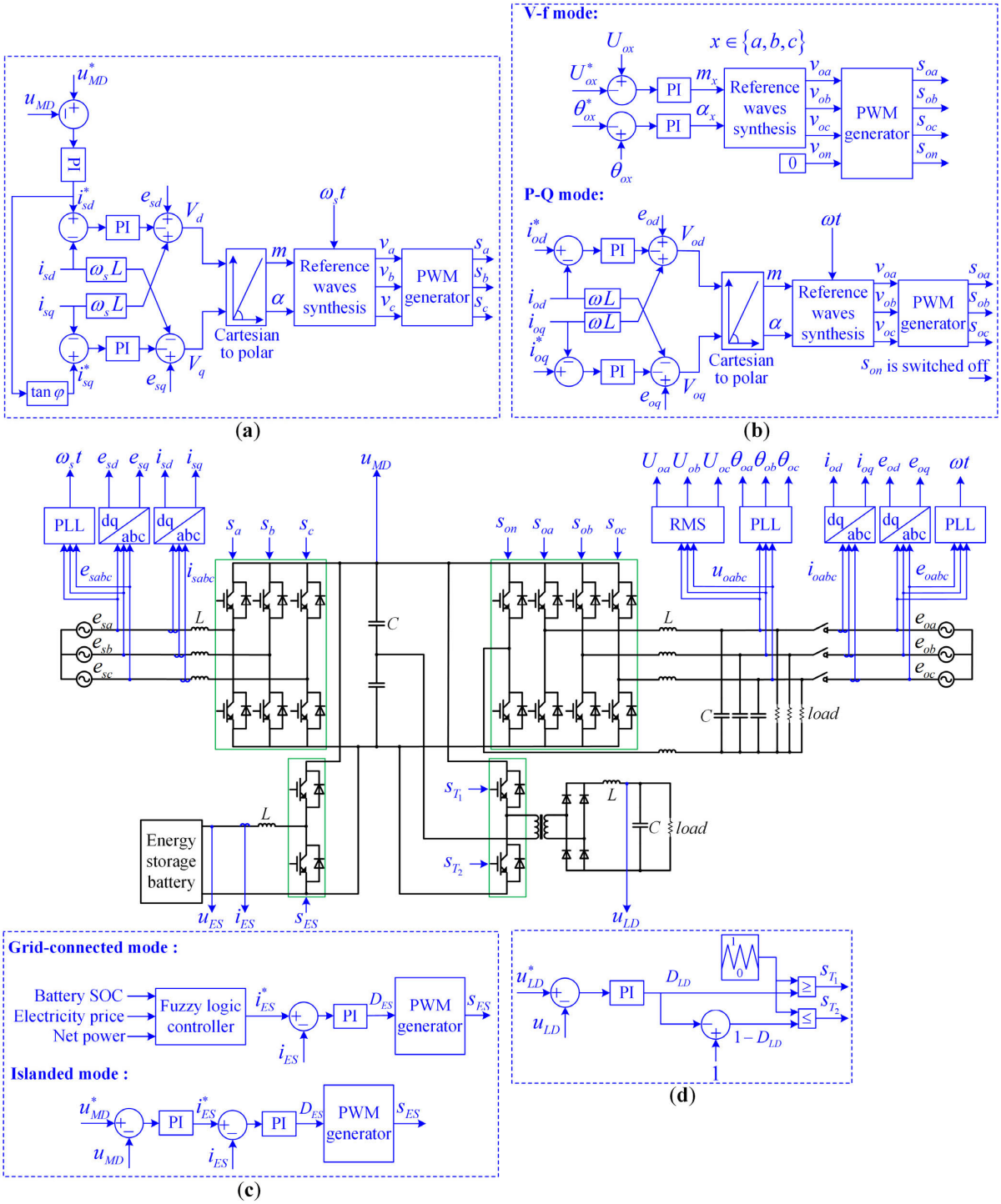


**FIGURE 4.** Main circuit of MER and corresponding main control strategy. (a) Control strategy of grid-connected part. (b) Control strategy of AC part. (c) Control strategy of ES part. (d) Control strategy of LV DC part.

In islanded mode, the port of grid-connected part is closed, and the controller of ES part is in charge of the voltage stability of MV DC link. There are two situations that cause a switch from grid-connected mode to islanded mode. One situation is called ''passive islanding'' when a failure occurs in the distribution grid, the other situation is called ''active islanding'' when an islanded command is sent out.

If a local fault occurs in AC part, ES part, or LV DC part, the MER will just block the fault part while the other normal parts will be unaffected. However, when an intolerable fault (e.g. overvoltage of MV DC bus, over temperature of radiator) is detected, the MER will enter fault mode and the protection system will take action to block all the ports of the MER. In fault mode, the MER will not enter standby mode unless

the fault is cleared and a reset command is received. It should be noted that the permissible fluctuation range of MV DC voltage is large enough (e.g., 0.9∼1.1 times rated voltage) to ensure that the MVDC voltage fluctuation will not exceed it in normal situations.

### B. MAIN CONTROL STRATEGY

The detailed main circuit configuration of MER and the corresponding main control strategy are illustrated in Fig. 4. As mentioned previously, there are five parts in the MER, and four converters are employed to guarantee regular operation. Since the MV DC bus decouples the other parts, the controllers of four converters are relatively independent. A three-phase half-bridge voltage source rectifier (VSR) with pulse width modulation (PWM) is employed in grid-connected part, and the DC side of VSR is connected to the MV DC part. A bidirectional DC/DC converter is selected in ES part to achieve the charge and discharge process of the ES battery. AC part adopts a three-phase four-leg inverter so as to supply power under unbalanced load condition, and LV DC part chooses a half-bridge DC/AC/AC/DC converter for its simplicity and economy in low-voltage small-capacity applications.

In grid-connected part, as shown in Fig. 4(a), the double closed-loop controller is employed in the three-phase PWM rectifier to maintain MV DC voltage at the rated value while getting sinusoidal input currents, including the outer loop for MV DC voltage and inner loop for grid currents which are converted into synchronous rotation d/q coordinate system. The reference value of the input current q-axis component $i_{sq}^{*}$ is set to zero by default to realize unity power factor, which is also allowed to be modified according to the desired power factor angle, so as to produce controllable reactive power.

In AC part, as shown in Fig. 4(b), the control strategies are different from the selected mode. If AC part works in V-f mode, the controller will comprise the root mean square (RMS) loop and phase angle loop for each phase voltage to supply the three-phase sinusoidal output voltages with constant frequency and constant amplitude, and the fourth leg will be controlled by high frequency PWM signals with 50% duty cycle to deal with unbalanced load. In this mode, if a microgrid is connected to the port of AC part, the grid-connected converter of microgrid is required to track the voltages generated by AC part. If AC part works in P-Q mode, AC part needs to track the voltages of the microgrid, and the closed-loop controller including d-axis and q-axis current loops is employed with current feed-forward decoupled mode to control the active power and reactive power at given values.

In ES part, as shown in Fig. 4(c), the bidirectional DC-DC converter in ES part adopts the two-switch mode where the upper and lower switch tubes are driven by complementary signals, since the two-switch mode is suitable for the applications where the power direction may change frequently. There are different control objectives for the controllers of ES part in grid-connected mode and islanded mode, and the bidirectional power flow is achieved by controlling the ES inductor voltage. In grid-connected mode, closed-loop control of ES inductor current is employed, and the ES battery charging/discharging current reference value is obtained by energy management strategy which will be discussed in later chapter. In islanded mode, ES part will replace grid-connected part to maintain the MV DC voltage at rated value, and the controller includes the outer MV DC voltage loop and inner ES inductor current loop.

In LV DC part, as shown in Fig. 4(d), the upper and lower bridge arms are switched on and switched off alternately with the same duty cycle, and the controller maintains the LV DC voltage at rated value by changing the duty cycle.

### C. MODE SWITCH STRATEGY

It is significant for the MER to achieve seamless transition between grid-connected mode and islanded mode. Unlike traditional microgrid [28], the MER allows power consumers to obtain AC power from the port of AC part, rather than the port of grid-connected part. If the MER switches from grid-connected mode to islanded mode, grid-connected part will be closed until the MER switches to grid-connected mode again. An advanced compensation strategy is employed to achieve seamless transition between grid-connected mode and islanded mode.

While the MER is switching from grid-connected mode to islanded mode, the stability of MV DC voltage will be controlled by the converter in ES part. To avoid the impacts on battery current and MV DC voltage during transition, voltage loop and inner current loop of ES part are calculated in advance, which can be expressed as (1) and (2), respectively.

$$I_{switch} = \frac{P_{switch}}{U_{bat}}, \tag{1}$$

$$D_{switch} = 1 - \frac{U_{bat}}{U_{MD}}, \tag{2}$$

where the $I_{switch}$ and $D_{switch}$ are the theoretical regular output values of the PI controllers in the outer MV DC voltage loop and inner ES inductor current loop, respectively. $U_{bat}$ and $U_{MD}$ are the average voltages of ES battery and MV DC part during the mode switching process, respectively. $P_{switch}$ is the net consumption power at the switching moment, which is equal to the difference between total load consumption power (from Port 3, Port 4 and Port 5) and total DERs generation power (from Port 3 and Port 4). It should be noted that the variation of DERs generation power is not considered in the mode switch strategy, since the time scale of mode switching process is much smaller than that of DERs generation power variation. Thus, it can be considered that $P_{switch}$ is constant during the mode switching process.

After calculation, the $I_{switch}$ and $D_{switch}$ are set as the initial output values of the PI controllers in the outer MV DC voltage loop and inner ES inductor current loop at the moment of switching, respectively.

While the MER is switching from islanded mode to grid-connected mode, the stability of MV DC voltage will be controlled by the converter in grid-connected part.

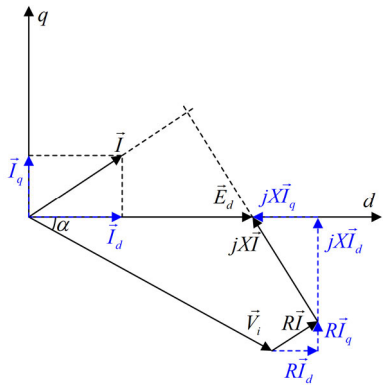


**FIGURE 5.** Vector diagram in the grid-connected part.

The converter in grid-connected part should be synchronized with the distribution grid and then the grid-connected part controller starts working [29], while the ES part controller switches to zero power transmission temporarily. To avoid the impacts on grid current and MV DC voltage during transition, the theoretical steady state output value of PI controllers in outer voltage loop and inner current loop of grid-connected part are calculated in advance. Taking the d-axis of the rotating coordinate system coincide with the three-phase grid voltage synthesis vector, and we can get

$$I_{d-switch} = \frac{P_{switch}}{3E_d}, \tag{3}$$

where the $I_{d-switch}$ is the theoretical steady state output values of the controller in the outer MV DC voltage loop, and $E_d$ is the grid voltage d-axis component.

Fig. 5 shows the vector diagram about the grid voltages and currents in the grid-connected part. According to Fig. 5, the theoretical steady state modulation ratio $m_{switch}$ and control angle $\alpha_{switch}$ can be expressed as (4) and (5), respectively.

$$m_{switch} = \frac{2\sqrt{2}\sqrt{\left(E_d + I_qX - I_dR\right)^2 + \left(I_qR + I_dX\right)^2}}{U_{MD}}, \tag{4}$$

$$\alpha_{switch} = \arctan\frac{I_qR + I_dX}{E_d + I_qX - I_dR}, \tag{5}$$

where the $I_d$ and $I_q$ are the grid current d-axis component and q-axis component, respectively. $R$ and $L$ are the values of resistance and inductance in the AC side of the grid-connected part, respectively.

Taking $I_{qref} = 0$, then $I_q = 0$ and $I_d = I_{d-switch}$ in the steady state. Generally, $I_dX$ is less than 0.1 $E_d$, so $(I_dX)^2$ is much smaller compared with $E_d^2$. In order to facilitate the calculation of digital signal processor in actual device, $(I_dX)^2$ can be ignored in equation (4) because $m_{switch}$ is not sensitive to the variation of $I_dX$. It should be noted that $I_dX$ cannot be ignored in equation (5) since $\alpha_{switch}$ is sensitive to the variation of $I_dX$. Based on (3), we can simplify (4) and (5) as (6) and (7), respectively. Then, (8) and (9) can be derived from (6) and (7).

$$m_{switch} = \frac{2\sqrt{2}\left(3E_d^2 - P_{switch}R\right)}{3E_dU_{MD}}, \tag{6}$$

$$\alpha_{switch} = \frac{P_{switch}X}{3E_d^2 - P_{switch}R}, \tag{7}$$

$$V_{d-switch} = E_d^* - m_{switch}\cos\alpha_{switch}, \tag{8}$$

$$V_{q-switch} = -m_{switch}\sin\alpha_{switch}, \tag{9}$$

where the $V_{d-switch}$ and $V_{q-switch}$ are the theoretical steady state output values of the PI controllers in the inner d-axis and q-axis grid current loops, respectively.

After calculation, the $I_{d-switch}$, $V_{d-switch}$ , and $V_{q-switch}$ are set as the initial output values of the PI controllers in the MV DC voltage loop, d-axis grid current loop, and q-axis grid current loop at the moment of switching, respectively.

## IV. ENERGY MANAGEMENT STRATEGY OF MER

In this section, the power flows in the grid-connected mode and islanded mode will be discussed, and the energy management strategy for grid-connected mode will be introduced in detail.

### A. DISCUSSION ON POWER FLOWS

The possible power flows of MER in grid-connected mode and islanded mode are shown in Fig. 6(a) and Fig. 6(b), respectively.

There are six cases (Case 1-6) of power flow directions in grid-connected mode, and the distinctions among the six cases are the different power flow directions of the grid-connected part power ($P_{GC}$) and ES part power ($P_{ES}$), which mainly depend on the SOC of ES battery ($SOC_{ESB}$), the electricity price of distribution grid ($EP$), and the difference between the total load demand ($P_{Load}$) and DER output ($P_{DER}$). For convenience of explanation, taking the direction of inflow into the MER as the positive direction.

Taking the $P_{Net}$ as the net output power, which can be expressed as (10).

$$P_{Net} = P_{DER} - P_{Load}, \tag{10}$$

where the $P_{Load}$ is added by the load consumption from MV DC part ($P_{MD}$), AC part ($P_{AC}$), and LV DC part ($P_{LD}$). $P_{DER}$ is added by the overall DGs output ($P_{DG}$), DESs power ($P_{DES}$) and microgrid power ($P_{MG}$). It should be mentioned that due to the high operating and on/off cost, the fuel cell will not be used in grid-connected mode.

Because the active power is balanced in the MER-based energy subnet, we can get

$$P_{Net} + P_{GC} + P_{ES} = 0. \tag{11}$$

The six cases of power flow directions in grid-connected mode are described in Table 1.

The typical examples shown in Table 1 take into account the $P_{Net}$, $EP$ and $SOC_{ESB}$. For example, in Case 1, $P_{Net} < 0$ means the load consumption is more than the power generated by DERs. Meanwhile, both $EP$ and $SOC_{ESB}$ are

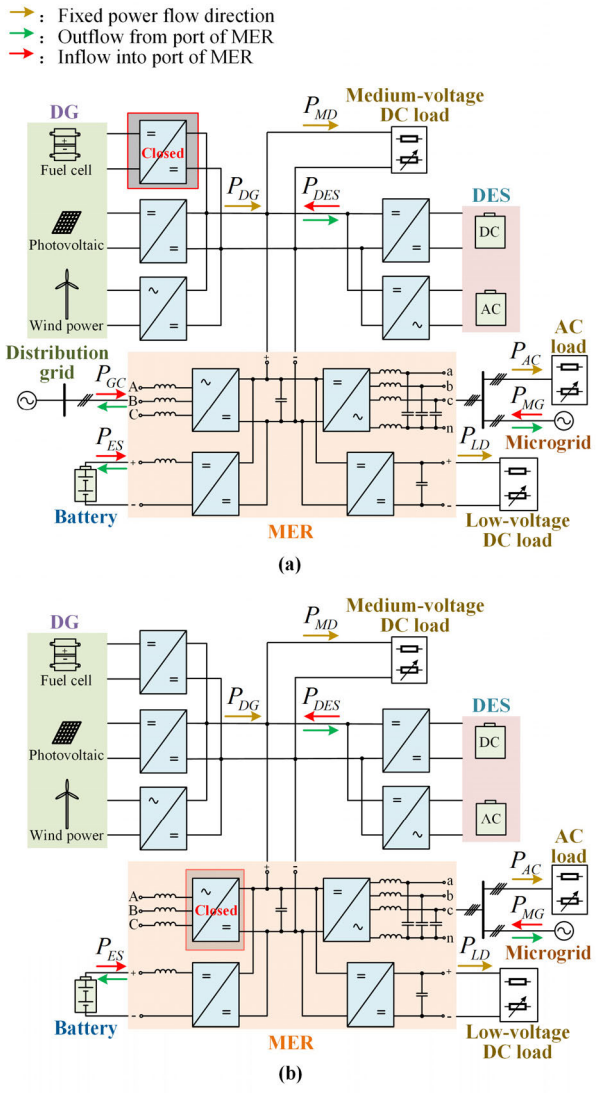


**FIGURE 6.** Power flows of MER. (a) In grid-connected mode. (b) In islanded mode.

**TABLE 1.** Possible power flow directions in grid-connected mode.

| Cases | Distinctions | |
|---|---|---|
| | Power flow directions | Typical examples |
| Case 1 | $P_{GC}>0$, $P_{ES}>0$ | $P_{Net}<0$, high EP and high SOC |
| Case 2 | $P_{GC}>0$, $P_{ES}=0$ | $P_{Net}<0$, high EP and low SOC, or low EP and high SOC |
| Case 3 | $P_{GC}>0$, $P_{ES}<0$ | $P_{Net}<0$, low EP and low SOC |
| Case 4 | $P_{GC}<0$, $P_{ES}>0$ | $P_{Net}>0$, high EP and high SOC |
| Case 5 | $P_{GC}<0$, $P_{ES}=0$ | $P_{Net}>0$, high EP and low SOC, or low EP and high SOC |
| Case 6 | $P_{GC}<0$, $P_{ES}<0$ | $P_{Net}>0$, low EP and low SOC |

relatively high. Then the ES battery should discharge to reduce the electricity bill. Table 1 will guide the formulation of energy management strategies in grid-connected mode.

In islanded mode, the ES battery is responsible for the active power balance of the MER-based energy subnet. Similar to (11), we can get

$$P_{Net}+P_{ES}=0. \tag{12}$$

If $P_{Net}<0$, it means that the ES battery is required to compensate the deficient power. In order to avoid the over discharge of battery, the fuel cell will supply power and the IPSs connected to non-essential loads will be disconnected if $SOC_{ESB}$ is below the lower threshold.

If $P_{Net}>0$, it means that there exist excess power to charge the ES battery. In order to avoid the over charge of battery, the IPSs connected to DGs will be disconnected if $SOC_{ESB}$ is above the upper threshold.

### B. ENERGY MANAGEMENT STRATEGY FOR GRID-CONNECTED MODE

In grid-connected mode, the energy management strategy is aimed to prolong battery life, improve economic benefits of power consumers, and smooth fluctuations of renewable energy production or load consumption. Based on Table 1, the desired charging/discharging current demand of ES battery ($I_{ESB}$) will depend on the three factors: $SOC_{ESB}$, $EP$, and $P_{Net}$. For convenience of analysis, assuming that both the purchasing electricity price and the selling electricity price are $EP$, and $I_{ESB}$ is positive when the ES battery discharges.

It is suitable to use fuzzy control [23] for the energy management strategy with multiple control objectives that are mutually restrictive. Therefore, a FLC is used to figure out the $I_{ESB}$. Considering that the rules of fuzzy controllers with more than two input variables are complex, it is expected to find a variable that can represent both $EP$ and $P_{Net}$. According to (11), $-P_{ES}-P_{Net}$ is equal to the grid transmitted power $P_{GC}$ in steady state. Considering that $EP$ times $P_{GC}$ to get unit-time electricity charge ($EC_{unit}$) of MER from the distribution network, which can reflect the economic benefits of power consumers and characterize the effects of $EP$ and $P_{Net}$ on $I_{ESB}$. For the purpose of calculating convenience, the normalized method is used to map $EP$ and $-P_{ES}-P_{Net}$ to the region [0, 1], then $EC_{unit}$ can be expressed as (13).

$$EC_{unit}=\frac{EP-EP_{\min}}{EP_{\max}-EP_{\min}}\times\left(\frac{P_{Rate}-P_{ES}-P_{Net}}{2P_{Rate}}\right), \tag{13}$$

where the $EP_{min}$ and $EP_{max}$ are the minimum and maximum electricity price over a day, respectively. $P_{Rate}$ is the rated capacity of grid-connected part.

It should be noted that the reason why $P_{GC}$ is not used in (13) directly is that $-P_{ES}-P_{Net}$ can contribute to smooth the fluctuations of renewable energy production or load consumption. If $P_{Net}$ changes, it will be reflected in $EC_{unit}$. Through the FLC, $P_{ES}$ will change in the opposite direction to compensate the variation of $P_{Net}$, thus suppressing power fluctuation on the grid side.

In the FLC, set $SOC_{ESB}$ and $EC_{unit}$ as the two input variables, and $I_{ESB}$ as the output variable. The range of $SOC_{ESB}$,

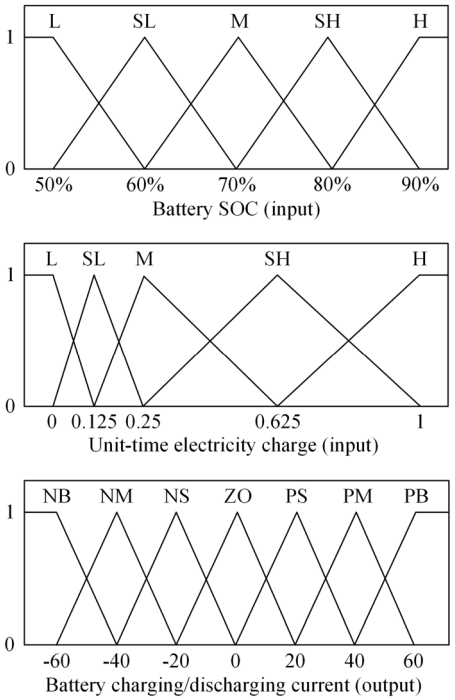


**FIGURE 7.** Membership functions of the input variables and output variable.

$EC_{unit}$, and $I_{ESB}$ are shown in (14).

$$\begin{cases} SOC_{ESB} \in [50\%, 90\%] \\ EC_{unit} \in [0, 1] \\ I_{ESB} \in [-60\text{A}, 60\text{A}]. \end{cases} \tag{14}$$

It should be noted that 50% is greater than the minimum allowable threshold of $SOC_{ESB}$, so as to ensure sufficient remaining capacity of ES battery to maintain the regular operation of MER when switching to islanded mode.

The membership functions of the input variables and output variable are shown in Fig. 7. Hereinto, five grades are employed to describe the input variables: L (low), SL (slightly low), M (medium), SH (slightly high), H (high). Meanwhile, seven grades are employed to describe the output variable: NB (negative big), NM (negative medium), NS (negative small), ZO (zero), PS (positive small), PM (positive medium), PB (positive big).

Table 2 shows the fuzzy control rules, which are designed according to the following basic criterions:

1) When $SOC_{ESB}$ is high, the charge of battery is not allowed. When $SOC_{ESB}$ is low, the discharge of battery is not allowed.

2) When $EC_{unit}$ is high, the power transmission from the MER to the distribution grid should be encouraged, and the charge of battery is not allowed. When $EC_{unit}$ is low, the power transmission from the distribution grid to the MER should be encouraged, and the discharge of battery is not allowed.

**TABLE 2.** Fuzzy control rules.

| $I_{ESB}$ | | $EC_{unit}$ | | | | |
|---|---|---|---|---|---|---|
| | | L | SL | M | SH | H |
| $SOC_{ESB}$ | L | NM | NS | ZO | ZO | ZO |
| | SL | NM | NS | ZO | ZO | PS |
| | M | NS | ZO | ZO | PS | PM |
| | SH | NS | ZO | PS | PM | PB |
| | H | ZO | ZO | PS | PB | PB |

**TABLE 3.** MER model parameters.

| Parameter | Value |
|---|---|
| Rated MER capacity | 30 kVA |
| Rated distribution grid voltage | 380 V |
| Rated AC frequency | 50 Hz |
| Rated MV DC-link voltage | 750 V |
| Rated AC part voltage | 380 V |
| Rated LV DC-link voltage | 48 V |
| Rated ES battery voltage | 220 V |
| Rated ES battery capacity | 10 Ah |
| Line inductance in grid-connected part | 1.5 mH |
| MV DC-link Capacitance | 15 mF |
| LC filter in AC part | 0.8 mH, 30 μF |
| Midline inductance in AC part | 0.4 mH |
| LC filter in LV DC part | 0.1 mH, 3300 μF |
| Rated ratio of the transformer in LV DC part | 6 : 1 |
| Filter inductance in ES part | 2 mH |
| Switching frequency of the converters | 6 kHz |

3) When $P_{Net} > 0$, the priority should be given to deliver surplus power to the distribution grid for economic benefit. Therefore, Table 2 is designed asymmetrically.

## V. SIMULATION AND EXPERIMENTAL RESULTS

### A. SIMULATION

In order to verify the proposed control and energy management strategies, a MER simulation model is established in MATLAB/SIMULINK, as shown in Fig. 8. The main circuit of the model is the same as that shown in Fig. 4. The ES battery adopts the lithium battery model, and the DGs employs the photovoltaic (PV) model, which consists of PV cells and a boost converter. Maximum power point tracking (MPPT) control algorithm is used in the PV model to fully utilize the PV output power. The main parameters are shown in Table 3.

1) *Case 1:* In this case, the effectiveness of mode switch strategy as well as the dynamic response of each port output when PV output power or load consumption power varies in a short time is investigated. For simplicity and without loss of generality, step changes of light intensity are used to simulate the variation of PV output power. The light intensity varies from 560 W/m$^2$ to 480 W/m$^2$ at 1 s, and to 400 W/m$^2$ at 2 s. Accordingly, the PV output power varies from 11.8 kW to 9.9 kW at 1 s, and to 8.1 kW at 2 s. The total load consumption power varies from 6 kW to 12 kW at 1.5 s. The distribution grid is set to fail at 0.5 s and recover at 2.5 s, and the battery charging current instruction value is set to 5 A in grid-connected mode.

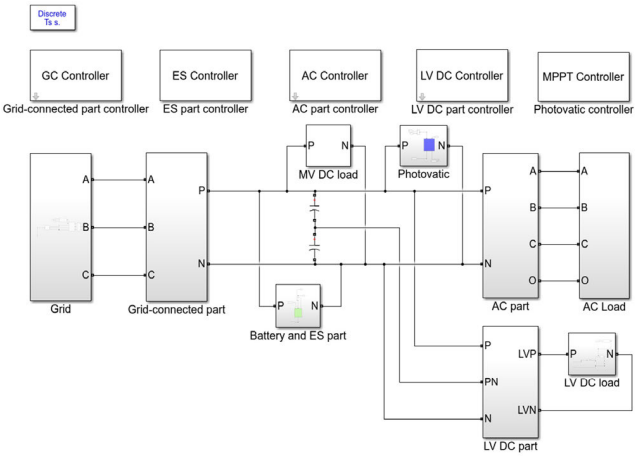


**FIGURE 8.** Simulation model of MER in MATLAB/SIMULINK.

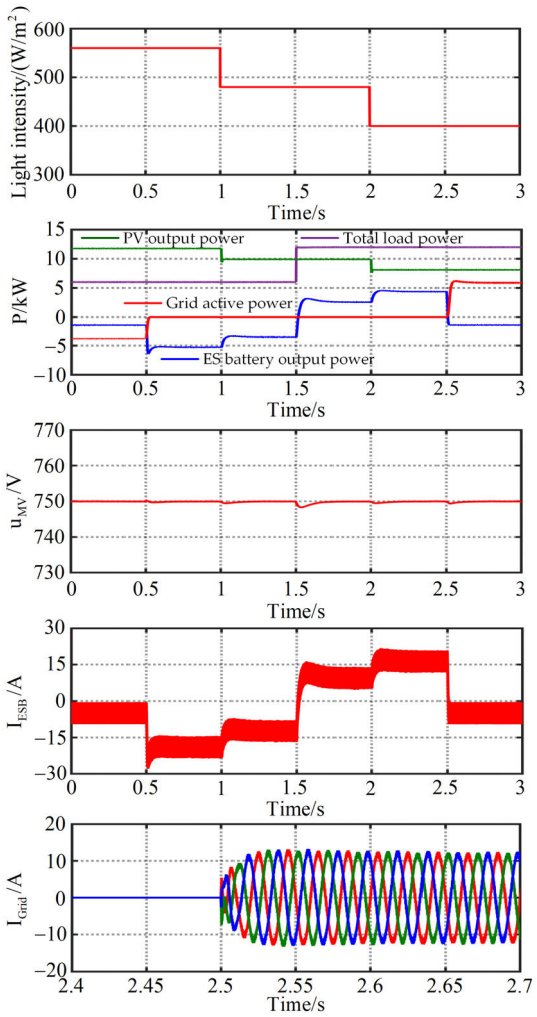


**FIGURE 9.** Simulation results of Case 1.

The simulation results are shown in Fig. 9. As can be seen, when the MER switches from grid-connected mode to islanded mode at 0.5 s, the active power balance of MER is maintained by ES part and the impact of $I_{ESB}$ is very light. When the MER switches from islanded mode to grid-connected mode at 2.5 s, the active power balance of MER is maintained by grid-connected part and the grid current has almost no impact. The transient process of the mode switching is very short and the MV DC-link voltage is unaffected. In addition, the variations of photovoltaic power generation and load power consumption have almost no influence on MV DC-link voltage. The simulation results shown in Fig. 9 validate the effectiveness of mode switch strategy.

2) *Case 2:* In this case, the effectiveness of energy management strategy for grid-connected mode is investigated. The MER works in grid-connected mode, while the PV output power and load consumption power change randomly over time, and *EP* (normalization value) varies from 0.7 to 0.3 at 2 s. The FLC employs the fuzzy control rules shown in Table 2.

Fig. 10(a) shows the simulation results when the initial $SOC_{ESB}$ is 80%, and Fig. 10(b) shows the simulation results when the initial $SOC_{ESB}$ is 60%. As can be seen, $SOC_{ESB}$ tend to change to the medium level (70%) for prolonging battery life. When *EP* and $P_{Net}$ change, the variation of $I_{ESB}$ is in the direction of improving economic benefits and smoothing power fluctuation of DER and load. As shown in Fig. 10(b), though $SOC_{ESB}$ is low, the priority is given to deliver surplus power to the distribution grid for economic benefit when $EC_{unit}$ is relatively high. The simulation results shown in Fig. 10 validate the effectiveness of energy management strategy for grid-connected mode.

### B. EXPERIMENTAL RESULTS

To verify the performance of the proposed control and energy management strategy in the actual device, a MER experimental prototype is designed and implemented, as shown in Fig. 11. The main circuit of the prototype is the same as that shown in Fig. 4, and the main parameters are the same as that shown in Table 3. As shown in Fig. 12, a programmable power supply device is employed to simulate renewable energy generation access to the MER. The laboratory test circuit is shown in Fig. 13.

Fig. 14 shows the MER experimental waveforms in steady state with 30 kW rated load. As shown in Fig. 14, the sinusoidal input currents and unity power factor are achieved, and the voltages of MV part, LV part, and AC part are maintained at each rated value, respectively.

Fig. 15 shows the MER experimental waveforms when switching on the 30 kW rated load. As shown in Fig. 15, though 30 kW load is switched on, the MV DC-link voltage has a minor fluctuation and restores stability quickly, and the voltages of AC part and LV DC part are unaffected.

Fig. 16 shows the MER experimental waveforms when the AC part is connected to a microgrid. As shown in Fig. 16, the microgrid input 7.5 kW active power to AC part while the MV DC part supply for 4.5 kW load, and the surplus power 3 kW is transmitted to the distribution grid.

Fig. 17 shows the MER experimental waveforms when switching between grid-connected mode and islanded mode. As shown in Fig. 17, during the transition from

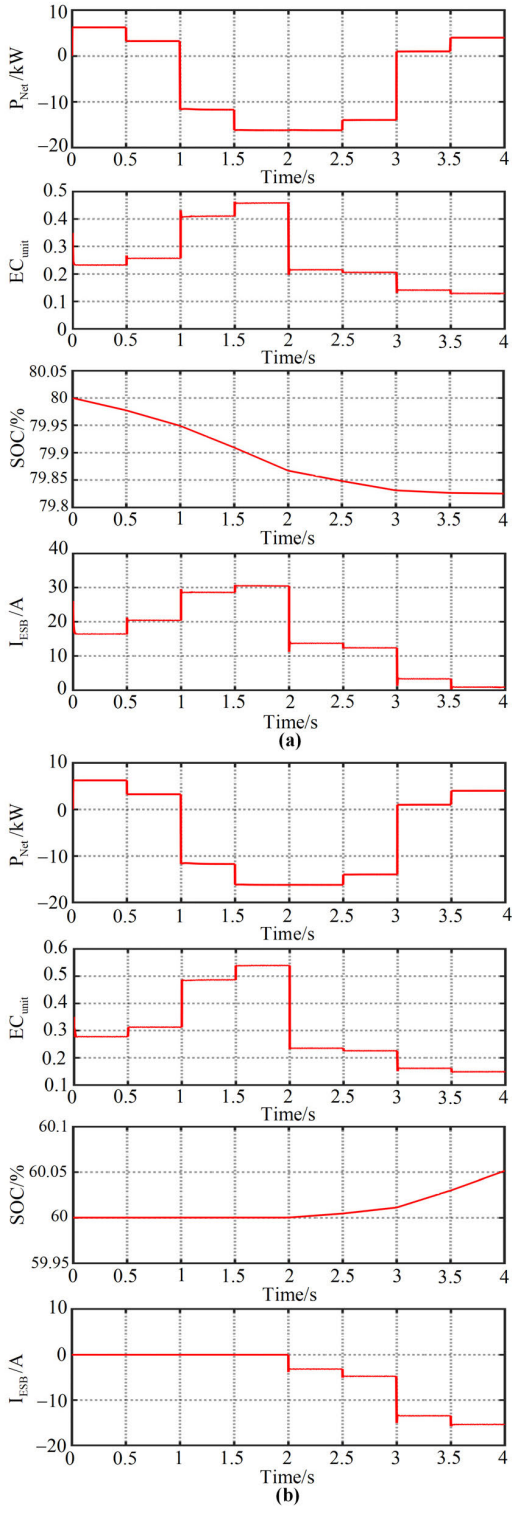


**FIGURE 10.** Simulation results of Case 2. (a) With 80% initial $SOC_{ESB}$. (b) With 60% initial $SOC_{ESB}$.

grid-connected mode to islanded mode, the ES part replaces the grid-connected part to control the MV DC-link voltage, and the impact of ES battery current is very light. And during the transition from islanded mode to grid-connected mode, the grid-connected part replaces the islanded part to control

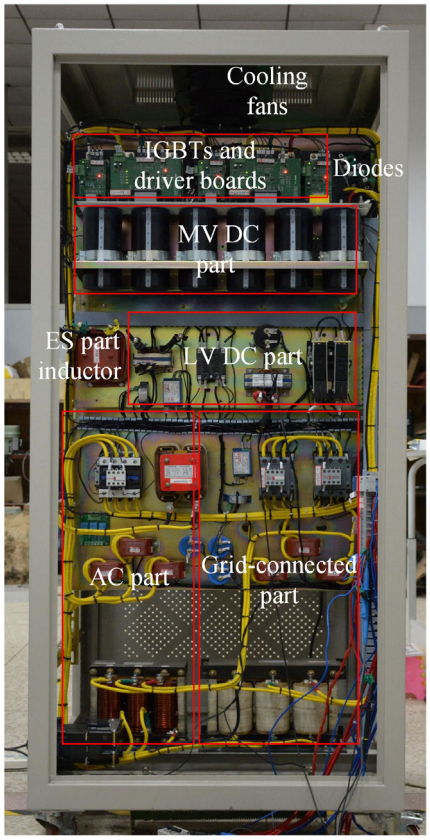


**FIGURE 11.** The MER experimental prototype.

**FIGURE 12.** The programmable power supply device.

the MV DC-link voltage, and the grid input currents have no impact. The voltages of MV DC part, AC part, and LV DC part are unaffected during the mode transition. The experimental results shown in Fig. 17 validate the effectiveness of mode switch strategy.

Fig. 18 shows the MER experimental waveforms under different input reactive power instruction values when the MER is in no-load condition. As shown in Fig. 18(a), the input reactive power instruction value is set to −14 kVar, and the grid current leads the grid voltage by 4.89 ms (88°). As shown

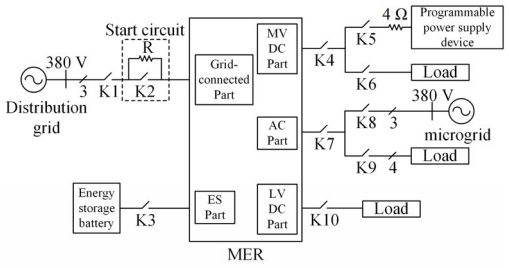


**FIGURE 13.** Laboratory test circuit.

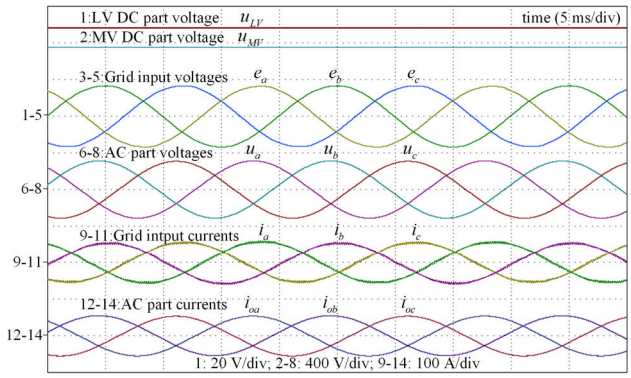


**FIGURE 14.** Experimental waveforms under loaded conditions.

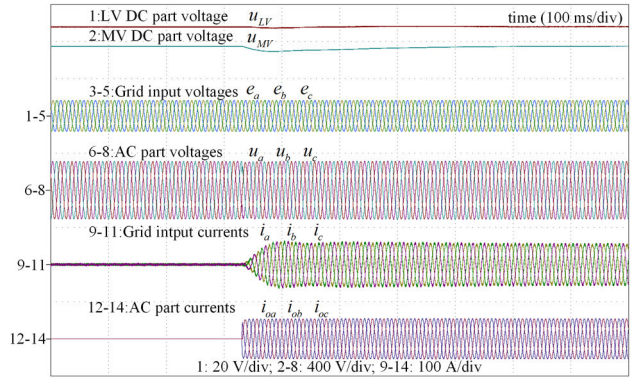


**FIGURE 15.** Experimental waveforms when switching on the load.

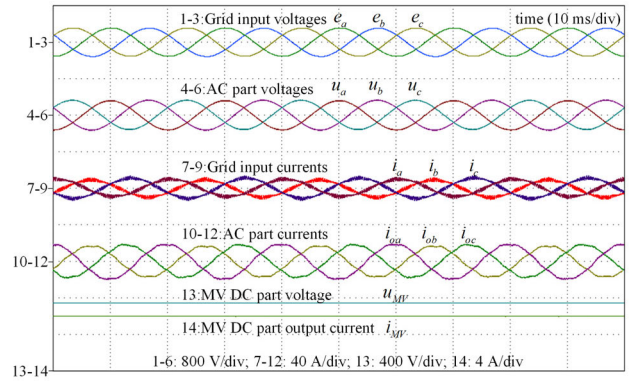


**FIGURE 16.** Experimental waveforms when AC part is connected to a microgrid.

in Fig. 18(b), the input reactive power instruction value is set to 14 kVar, and the grid current lags the grid voltage by 5.06 ms (91°). The experimental results shown in Fig. 18

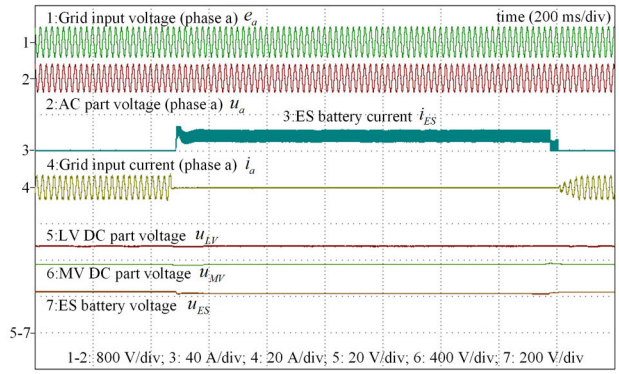


**FIGURE 17.** Experimental waveforms when switching between grid-connected mode and islanded mode.

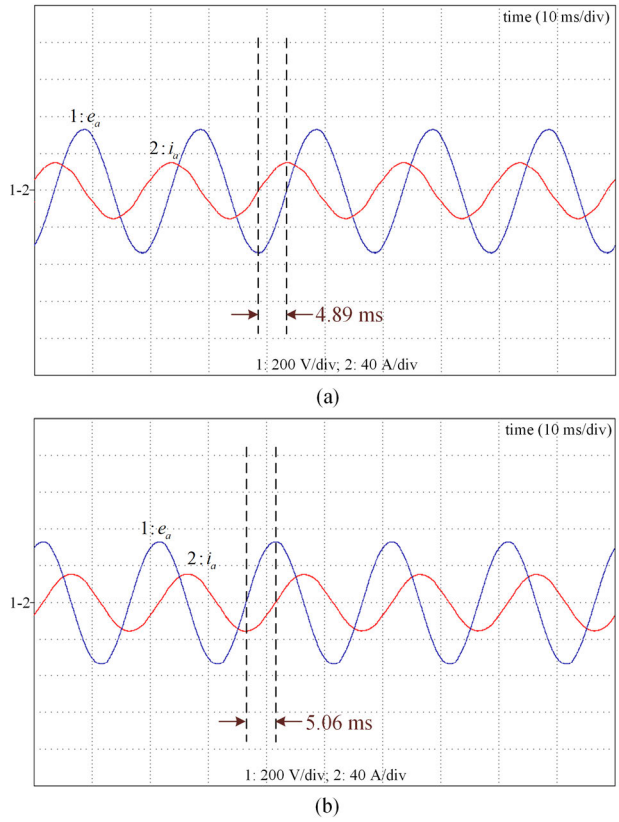


**FIGURE 18.** Experimental waveforms with different input reactive power instruction values. (a) Leading reactive power. (b) Lagging reactive power.

demonstrate that the MER has the function of reactive power compensation.

Fig. 19 shows the MER experimental waveforms when the programmable power supply device is connected to the MV DC part. It should be noted that a filter ($f_c = 100$ Hz) is added to the recording channel of ES battery current so as to see the current variation more intuitively. By importing the experimental data into MATLAB/SIMULINK for processing, the corresponding power curves of grid-connected part, ES part, and MV DC part are plotted in Fig. 20. For simplicity, the step changing output power from the programmable power supply device is used to simulate the

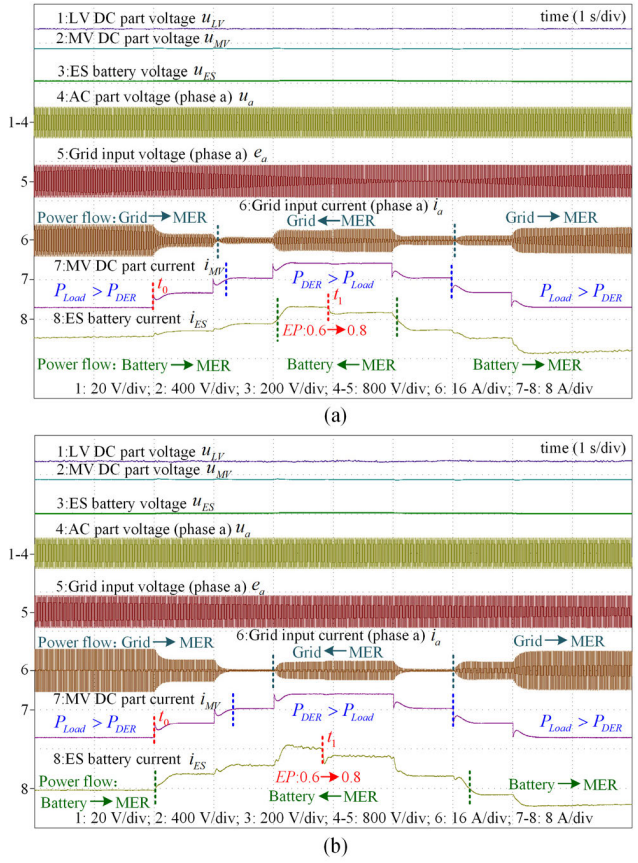


**FIGURE 19.** Experimental waveforms when the programmable power supply device is connected to MV DC part. (a) With relatively high initial $SOC_{ESB}$. (b) With relatively low initial $SOC_{ESB}$.

fluctuation of renewable energy generation (e.g. PV output with varying illumination intensity), and the ES battery voltage is employed to replace $SOC_{ESB}$ as an input variable of the FLC mentioned previously.

Fig. 19(a) shows the experimental waveforms when the initial $SOC_{ESB}$ is relatively high (the initial open circuit voltage of battery is 216 V). The MV DC port is connected with 4.1 kW load at first, and the programmable power supply device starts to produce step changing output power at $t_0$. As shown in Fig. 20(a), the net output power varies from −4.1 kW to 2.6 kW step by step and then back to −4.1 kW step by step again, and the ES battery power changes in the direction of smoothing the fluctuation of renewable energy generation. At $t_1$, $EP$ is set to vary from 0.6 to 0.8, and it can be seen that the ES battery charging power is reduced to improve economic benefits.

For a comparison, Fig. 19(b) shows the experimental waveforms when the initial $SOC_{ESB}$ is relatively low (the initial open circuit voltage of battery is 202 V). Except for the initial $SOC_{ESB}$, the other experimental conditions are the same as those described for Fig. 19(a). Comparing Fig. 20(a) and Fig. 20(b), it can be seen that the ES battery in low $SOC_{ESB}$ state increases charging power and decreases discharging power compared with that in high $SOC_{ESB}$ state,

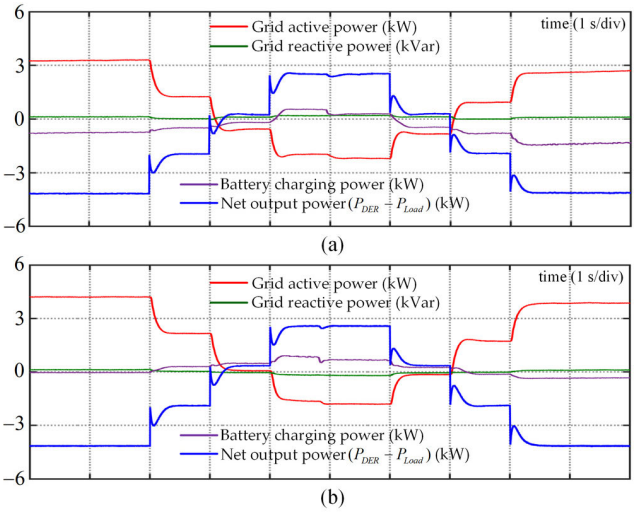


**FIGURE 20.** Power curves of grid-connected part, ES part, and MV DC part when the programmable power supply device is connected to MV DC part. (a) With relatively high initial $SOC_{ESB}$. (b) With relatively low initial $SOC_{ESB}$.

so the $SOC_{ESB}$ can be maintained within a reasonable range. The experimental results shown in Fig. 19 and Fig. 20 validate the effectiveness of energy management strategy for grid-connected mode.

## VI. CONCLUSIONS

This paper introduces a MER which is applicable for low-voltage distribution network. The MER has lots of advantages, including the plug-and-play access of DERs and loads, various forms of electric energy, unified control and management of the MER-based energy subnet, high power supply reliability, fault isolation between the grid side and the users side, etc. Corresponding coordinated control strategies are developed to guarantee the regular operation of MER, and to achieve seamless transition between grid-connected mode and islanded mode. The energy management strategies are proposed for grid-connected mode to obtain the desired charging/discharging state of energy battery by a FLC, which is aimed to prolong battery life, to improve economic benefits of power consumers, and to smooth fluctuations of renewable energy production or load consumption. The simulation and experimental results have validated the coordinated control and energy management strategies.

The implementation of an MER experimental prototype proves that the MER is applicable for low-voltage distribution network. With the reduction of device volume and cost, it is promising to achieve the widespread application of MER in low-voltage distribution network, which will be an essential step for future EI construction.

## REFERENCES

[1] A. Q. Huang, M. L. Crow, G. T. Heydt, J. P. Zheng, and S. J. Dale, "The future renewable electric energy delivery and management (FREEDM) system: The energy Internet," *Proc. IEEE*, vol. 99, no. 1, pp. 133–148, Jan. 2011.

[2] K. Wang, J. Yu, Y. Yu, Y. Qian, D. Zeng, S. Guo, Y. Xiang, and J. Wu, "A survey on energy Internet: Architecture, approach, and emerging technologies," *IEEE Syst. J.*, vol. 12, no. 3, pp. 2403–2416, Sep. 2018.

[3] A. Luo, Q. Xu, F. Ma, and Y. Chen, "Overview of power quality analysis and control technology for the smart grid," *J. Mod. Power Syst. Clean Energy*, vol. 4, no. 1, pp. 1–9, Jan. 2016.

[4] J. Miao, N. Zhang, C. Kang, J. Wang, Y. Wang, and Q. Xia, "Steady-state power flow model of energy router embedded AC network and its application in optimizing power system operation," *IEEE Trans. Smart Grid*, vol. 9, no. 5, pp. 4828–4837, Sep. 2018.

[5] A. Kordonis, R. Takahashi, D. Nishihara, and T. Hikihara, "The three-phase power router and its operation with matrix converter toward smart-grid applications," *Energies*, vol. 8, no. 4, pp. 3034–3046, Apr. 2015.

[6] R. Abe, H. Taoka, and D. McQuilkin, "Digital grid: Communicative electrical grids of the future," *IEEE Trans. Smart Grid*, vol. 2, no. 2, pp. 399–410, Jun. 2011.

[7] Y. Xu, J. Zhang, W. Wang, A. Juneja, and S. Bhattacharya, "Energy router: Architectures and functionalities toward energy Internet," in *Proc. IEEE Int. Conf. Smart Grid Commun.*, Brussels, Belgium, Oct. 2011, pp. 31–36.

[8] S. Hambridge, A. Q. Huang, and R. Yu, "Solid state transformer (SST) as an energy router: Economic dispatch based energy routing strategy," in *Proc. IEEE Energy Convers. Congr. Expo. (ECCE)*, Montreal, QC, Canada, Sep. 2015, pp. 2355–2360.

[9] S. Zhao, Z. Wang, J. Umuhoza, A. Mantooth, Y. Zhao, and C. Farnell, "Distributed power quality enhancement using residential power routers," in *Proc. IEEE Appl. Power Electron. Conf. Expo. (APEC)*, San Antonio, TX, USA, Mar. 2018, pp. 513–520.

[10] L. Yuan, S. Wei, J. Ge, Z. Zhao, and R. Huang, "Design and implementation of AC-DC hybrid multi-port energy router for power distribution networks," in *Proc. 18th Int. Conf. Elect. Mach. Syst. (ICEMS)*, Pattaya, Thailand, Oct. 2015, pp. 591–596.

[11] P. H. Nguyen, W. L. Kling, and P. F. Ribeiro, "Smart power router: A flexible agent-based converter interface in active distribution networks," *IEEE Trans. Smart Grid*, vol. 2, no. 3, pp. 487–495, Sep. 2011.

[12] X. She, A. Q. Huang, S. Lukic, and M. E. Baran, "On integration of solid-state transformer with zonal DC microgrid," *IEEE Trans. Smart Grid*, vol. 3, no. 2, pp. 975–985, Jun. 2012.

[13] Y. Kado, D. Shichijo, K. Wada, and K. Iwatsuki, "Multiport power router and its impact on future smart grids," *Radio Sci.*, vol. 51, no. 7, pp. 1234–1246, Jul. 2016.

[14] M. Gao, K. Wang, and L. He, "Probabilistic model checking and scheduling implementation of an energy router system in energy Internet for green cities," *IEEE Trans Ind. Informat.*, vol. 14, no. 4, pp. 1501–1510, Apr. 2018.

[15] M. R. Sandgani and S. Sirouspour, "Coordinated optimal dispatch of energy storage in a network of grid-connected microgrids," *IEEE Trans. Sustain. Energy*, vol. 8, no. 3, pp. 1166–1176, Jul. 2017.

[16] Q. Duan, W. Sheng, X. Meng, C. Shi, J. Wang, Z. Ji, and Z. Lv, "Research on energy sub grid for the future energy Internet," *Proc. CSEE*, vol. 36, no. 2, pp. 388–398, Jan. 2016.

[17] B. Liu, J. Chen, Y. Zhu, Y. Liu, and Y. Shi, "Distributed control strategy of a microgrid community with an energy router," *IET Gener., Transmiss. Distrib.*, vol. 12, no. 17, pp. 4009–4015, Sep. 2018.

[18] Y. Liu, Y. Fang, and J. Li, "Interconnecting microgrids via the energy router with smart energy management," *Energies*, vol. 10, no. 9, p. 1297, Aug. 2017.

[19] Z. Li, P. Li, W. Sheng, S. Du, Q. Duan, and Z. Lv, "Research on a household energy router for energy Internet," in *Proc. 13th IEEE Conf. Ind. Electron. Appl. (ICIEA)*, Wuhan, China, May/Jun. 2018, pp. 952–957.

[20] J. M. Rodriguez-Bernuz, E. Prieto-Araujo, F. Girbau-Llistuella, A. Sumper, R. Villafafila-Robles, and J. A. Vidal-Clos, "Experimental validation of a single phase intelligent power router," *Sustain. Energy, Grids Netw.*, vol. 4, pp. 1–15, Dec. 2015.

[21] L. Olatomiwa, S. Mekhilef, M. S. Ismail, and M. Moghavvemi, "Energy management strategies in hybrid renewable energy systems: A review," *Renew. Sustain. Energy Rev.*, vol. 62, pp. 821–835, Sep. 2016.

[22] F. J. Vivas, A. De las Heras, F. Segura, and J. M. Andújar, "A review of energy management strategies for renewable hybrid energy systems with hydrogen backup," *Renew. Sustain. Energy Rev.*, vol. 82, pp. 126–155, Feb. 2018.

[23] Y.-K. Chen, Y.-C. Wu, C.-C. Song, and Y.-S. Chen, "Design and implementation of energy management system with fuzzy control for DC microgrid systems," *IEEE Trans. Power Electron.*, vol. 28, no. 4, pp. 1563–1570, Apr. 2013.

[24] S. Berrazouane and K. Mohammedi, "Parameter optimization via cuckoo optimization algorithm of fuzzy controller for energy management of a hybrid power system," *Energy Convers. Manage.*, vol. 78, pp. 652–660, Feb. 2014.

[25] M. Hosseinzadeh and F. R. Salmasi, "Power management of an isolated hybrid AC/DC micro-grid with fuzzy control of battery banks," *IET Renew. Power Gener.*, vol. 9, no. 5, pp. 484–493, Jul. 2015.

[26] Y. Liu, J. Li, Y. Wu, and F. Zhou, "Coordinated control of the energy router-based smart home energy management system," *Appl. Sci.*, vol. 7, no. 9, p. 943, Sep. 2017.

[27] M. H. Athari and M. M. Ardehali, "Operational performance of energy storage as function of electricity prices for on-grid hybrid renewable energy system by optimized fuzzy logic controller," *Renew. Energy*, vol. 85, pp. 890–902, Jan. 2016.

[28] J. Rocabert, A. Luna, F. Blaabjerg, and P. Rodriguez, "Control of power converters in AC microgrids," *IEEE Trans. Power Electron.*, vol. 27, no. 11, pp. 4734–4749, Nov. 2012.

[29] A. Micallef, M. Apap, C. Spiteri-Staines, and J. M. Guerrero, "Single-phase microgrid with seamless transition capabilities between modes of operation," *IEEE Trans. Smart Grid*, vol. 6, no. 6, pp. 2736–2745, Nov. 2015.

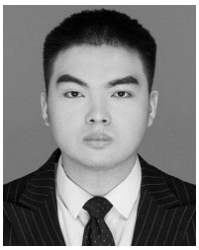

**BIN LIU** received the B.S. degree in electrical engineering from the Huazhong University of Science and Technology, Wuhan, China, in 2015, where he is currently pursuing the Ph.D. degree with the State Key Laboratory of Advanced Electromagnetic Engineering and Technology, School of Electrical and Electronic Engineering.

His research interest includes the application of power electronic technology in power systems.

**WEIHAN WU** received the B.S. degree from the Huazhong University of Science and Technology, Wuhan, China, in 2017, where he is currently pursuing the M.S. degree with the State Key Laboratory of Advanced Electromagnetic Engineering and Technology, School of Electrical and Electronic Engineering.

His research interests include new energy resources, energy storage, and microgrid.

**CHUNXIAO ZHOU** received the B.S. degree in electrical engineering from the Huazhong University of Science and Technology, Wuhan, China, in 2017, where he is currently pursuing the M.S. degree with the State Key Laboratory of Advanced Electromagnetic Engineering and Technology, School of Electrical and Electronic Engineering.

His research interests include power electronics, power systems, and real-time emulation platforms.

**CHENGXIONG MAO** (M'93–SM'08) received the B.S., M.S., and Ph.D. degrees from the Department of Electrical Engineering, Huazhong University of Science and Technology (HUST), in 1984, 1987, and 1991, respectively.

He was a Visiting Scholar with the University of Calgary, Calgary, AB, Canada, from January 1989 to January 1990, and also with Queen's University Belfast, Belfast, U.K., from December 1994 to December 1995. He was conducting research at Technische Universitaet Berlin, Berlin, Germany, from April 1996 to April 1997 with the support of Humboldt Foundation. He is currently a Professor with HUST. His current research interests include power system operation and control, the excitation control of synchronous generator, and the applications of high power electronic technology to power systems.

**DAN WANG** (M'07–SM'17) received the B.S., M.S., and Ph.D. degrees from the Department of Electrical Engineering, Huazhong University of Science and Technology (HUST), Wuhan, China, in 1999, 2002, and 2006, respectively.

He was a Postdoctoral Researcher, from 2006 to 2008, sponsored by the China Postdoctoral Science Foundation in Department of Control Science and Engineering, HUST. From 2008 to 2009, he was a Visiting Research Associate with the Department of Electrical and Computer Engineering, Michigan State University, USA. In 2008, he joined HUST, where he is currently a Professor. His research interests include power system operations and control, and power conditioning and grid-connection of alternative energy sources.

**QING DUAN** received the M.S. degree from the Huazhong University of Science and Technology, Wuhan, China, in 2004, and the Ph.D. degree from Shandong University, Jinan, China, in 2010.

He was a Visiting Scholar with Arizona State University, Tempe, Arizona, USA, from 2017 to 2018. He is currently a Senior Engineer with the Power Distribution Department, China Electric Power Research Institute, Beijing. His research interests include power electronics technologies, power distribution grid systems, and Energy Internet.

**GUANGLIN SHA** received the B.S. degree in electrical engineering and the Ph.D. degree in power electronics from the China University of Mining and Technology, Beijing, China, in 2011 and 2016, respectively.

Since 2016, he has been an Electrical Engineer with the Power Distribution Department, China Electric Power Research Institute, Beijing. His research interests include bidirectional isolated dc/dc converters, power electronics transformer, energy router, and ac/dc hybrid distribution systems.